

RESEARCH

Synthesis, Characterization and Humidity Sensing Application of Perovskite LaFeO₃

Avadhesh Kumar Yadav^{1,*} 

¹Department of Physics
F.A.A. Govt. PG College
Mahmudabad,
Sitapur 261203 (India)
(An Associated College of
University of Lucknow,
Lucknow)

*Corresponding author:
E-mail: yadav.av11@gmail.com
Tel.: 9454195697
Avadhesh Kumar Yadav

Web of Science Researcher ID:
AAI-2004-2019

ABSTRACT

In the past few decades, lanthanum ferrite has grown the importance in research due to attractive LPG/ humidity sensing and photolytic applications. In present study, the perovskite lanthanum ferrite was synthesized via solid state reaction route for three compositions by varying La/Fe ratio. The synthesized samples were characterized by Fourier transform spectroscopy, UV-vis spectroscopy, X-ray diffraction and scanning electron microscopy. The crystallization of lanthanum ferrite is confirmed by X-ray diffraction studies. The average crystallite size was found to be 45-50 nm. Surface morphological study of synthesized samples shows the uniform growth of the particles and grain which leaves the pores during its inter connection. These pores act as gas adsorption sites. The optical band gap of synthesized LaFeO₃ samples were found to be 3.91-4.03 eV. Prepared samples were investigated for humidity sensing application. The average sensitivity of synthesized lanthanum ferrite samples was found to be 10.18-11.46 MΩ/%RH. The average sensitivity varies with the composition of the sample.

KEYWORDS

Lanthanum ferrite, X-ray diffraction, Scanning electron microscopy, UV-vis spectroscopy, Humidity sensor.

INTRODUCTION

The concentration of water vapors available in the air, called as humidity, plays a significant role in various sectors like sugar and paper based industries, chemicals and medicine industries, automotive industries, climatology, heating ventilation and air conditioning (HVAC) systems, agriculture [1]. The monitoring of humidity levels in several industries plays a potential role due to their possible effects on manufacturing and products. Thus the detection of humidity becomes important to fulfil the purpose of its monitoring. Moreover, the humidity is also important in human breaths because some diseases require more controlled relative humidity. Humidity sensors become a special attraction of importance in research after COVID-19 and reduced the risk of bacterial transmission associated with conventional touch displays [2-4].

The perovskite type ferrite ceramics materials have attracted significant interest for potential applications in humidity sensors due to its ability to withstand exacting

physical and chemical conditions. The perovskite ferrite has the general formula ABO₃, where A and B are lanthanide/alkali earth element and transition metal, respectively. Lanthanum ferrite has received growing attention due to its wide range of application in biosensors, chemical sensors, optical and ferroelectric properties. It is synthesized by mechanochemical, hydrothermal process, auto-combustion method, co-precipitation, microwave assisted synthesis and solid state reaction route. The control on shape, size and surface of lanthanum ferrite ceramic is a key factor for humidity sensing research [5-9].

In present investigation, the lanthanum ferrite was synthesized via solid state reaction route. This method does not require the costly raw materials and it is one of the simplest synthesis route. The main requirement of solid state reaction method is high sintering temperature which improves crystallization, porosity and grains in comparison to starting particles. The microstructure of ferrites in solid state reaction route may be divided in three stages of surface, lattice and grain boundaries

diffusion. High oxidation reduction and electrical conductivity of perovskite LaFeO_3 is very important for electrochemical applications. It has a stable crystal structure, good thermal stability and inherent property of containing oxygen vacancies. Ferrite sensors are preferred due to its large surface area, uniform grain size and nanostructure which have to a large surface phenomenon. This effect is suitable for humidity sensing applications. The humidity sensing materials are improving their sensing response, response and recovery times with low hysteresis and high stability. Most humidity sensors are based either on resistance or capacitance. The absorption of water molecules on the nano material surface is reflected in an impedance of dielectric constant change. The increase in surrounding humidity reduces the resistivity of the ferrite nanoparticles. The humidity is specified as relative humidity (RH) which indicates the amount of water vapors at a specified temperature [10].

Lanthanum Ferrite samples were prepared by solid state reaction route. The synthesized samples were studied for crystallographic, microstructure and optical properties. The samples were further tested for humidity sensing applications. The humidity sensing behavior of lanthanum ferrite nanostructure was studied in a wide range of relative humidity (10-99%RH). The sensing studies revealed that lanthanum ferrite shows good average sensitivity which lies in the range 10.18-11.46 $\text{M}\Omega/\%RH$.

EXPERIMENTAL

Materials

Analytical grade chemical lanthanum carbonate and ferric carbonate are used as raw materials. Mentioned chemicals are purchased from HiMedia Mumbai, Maharashtra, India having purity more than 99.5%.

Material synthesis

Perovskite lanthanum ferrite was prepared by solid state reaction route method using high grade chemicals ferric carbonate (HiMedia) and lanthanum carbonate (HiMedia), purity is higher than 99.5%. The raw ingredients were grounded via mortar and pestle in acetone media. The grounded fine powder was calcined in a muffle furnace at temperature 800°C for 5 h. to improve purity by removal of carbonate in the form of CO_2 . The calcined powder was re-grounded using mortar and pestle. The grounded fine powder was used for pelletization in KBR media using a hydraulic press machine (City instruments, New Delhi, India) at uniaxial pressure 650 MPa. The fabricated pellets were sintered at 1000°C for 5 h. The complete synthesis process can be understood by schematic diagram **Fig. 1**. Lanthanum ferrite samples were prepared in three basic compositions (1) 45 weight percentage of La_2O_3 and 55 weight percentage of Fe_2O_3 (LF1), (2) 50 weight percentage of La_2O_3 and 50 weight percentage of Fe_2O_3 (LF2), and (3) 55 weight percentage of La_2O_3 and 45 weight percentage of Fe_2O_3 (LF3).

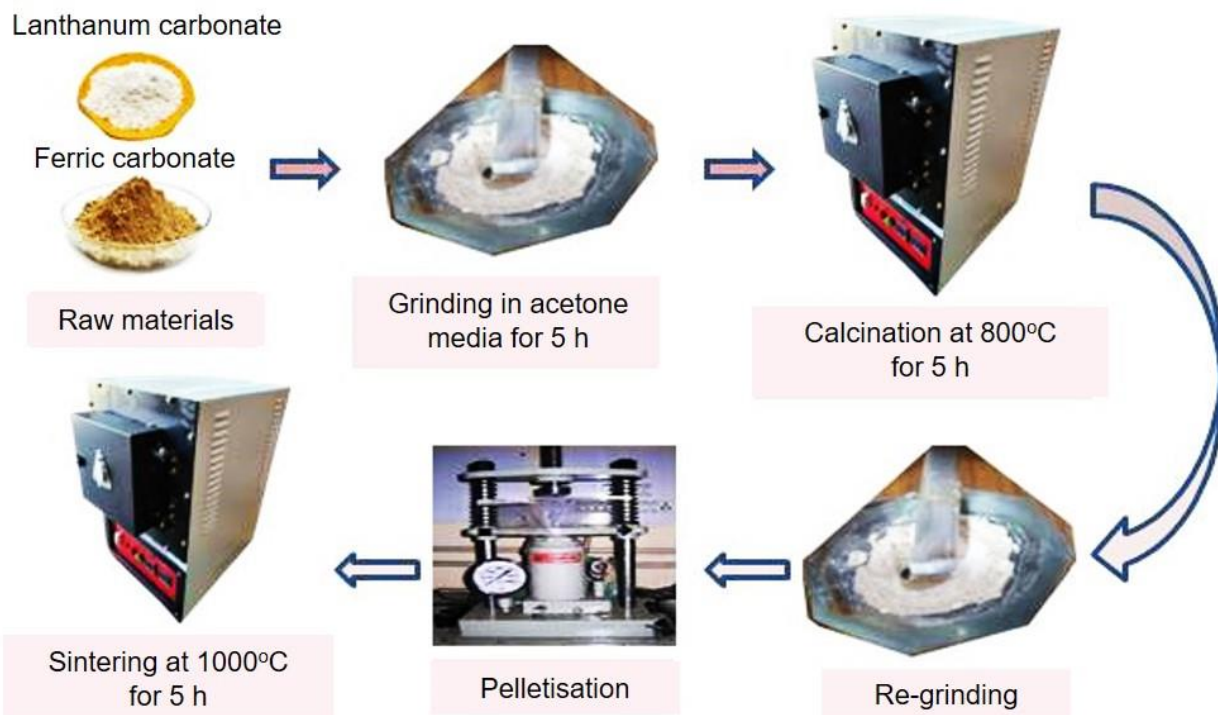


Fig. 1. Schematic diagram of synthesis of lanthanum ferrite via solid state reaction route.

Characterizations

The Molecular and bonding characteristics of prepared lanthanum ferrite samples were studied by Fourier transform infrared spectrum (FTIR). FTIR data was recorded with Fourier transform infrared spectrometer (FTIR) employing Shimadzu-8400S spectrophotometer over the range of 4000 to 400 cm^{-1} . The optical properties like optical band gap of each prepared samples were analyzed by data recorded by UV-vis absorption spectrophotometer (Model- V670, Jasco) in UV and visible ranges from 200-800 nm. The optical band gap was calculated by Tauc plot. The prepared samples were characterized for crystallographic analysis using X-ray diffraction (XRD) employing Rigaku Miniflex-II X-ray diffractometer using $\text{Cu-K}\alpha_1$ radiation having wavelength $\lambda = 1.5406 \text{ \AA}$. XRD data were measured in terms of intensity in diffraction angle range of $20\text{--}80^\circ$. The average crystallite size of powdered samples was calculated by Debye-Scherrer formula. The surface morphology of a well prepared sample was examined using a scanning electron microscope, SEM, (model LEO 430 Cambridge Instruments Ltd. UK). In analyzing the surface morphology, the sample prepared follows several steps. The prepared pellet samples were well polished by 100, 600, 1000 mesh SiC powder as well as 1/0, 2/0, 3/0 and 4/0 grades sand paper. The polished samples were etched with 30% $\text{HNO}_3 + 20\%$ HF solution and further coated with silver-palladium (Poraton Sc-7640 Sputter).

For the humidity sensing a special humidity chamber was designed which consists of an Ag-pellet-Ag electrode system well connected to the protruding electrodes of the electrometer. For measuring the resistance of the sensing pellet sample two silver electrodes were grown on opposite ends of the alumina substrate. Humidity chamber used in this investigation consists of a steel container having an air tight and movable glass lid to cover it. Two glass bowls were kept inside it one by one; one contains saturated aqueous solution of KOH to dehumidify the chamber up to 10%RH and other contains saturated aqueous solution of K_2SO_4 to humidify the chamber up to 95%. Pellet sample was put within this system and sensing measurements were performed. Variations in humidity inside the chamber were recorded by a standard hygrometer associated with a thermometer (Huger, Germany) and corresponding variations in electrical resistance were measured by Keithley Electrometer (Model 6514A). The least count of hygrometer used here was 1%RH.

RESULTS AND DISCUSSION

FTIR Spectroscopy

Fourier Transform Infrared (FTIR) spectra of well synthesized lanthanum ferrite samples are shown in Fig. 2(a-c). Spectra clearly indicates formation of several transmission bands. The presence of O-H bonding of

adsorbed water in each prepared samples were confirmed by the strong bands at 3610 and 3448 cm^{-1} [11]. The bands arise near 2928 and 2857 cm^{-1} are attributed to the C-H stretching bands, i.e. hydrogen bonding [12-13]. C=O vibration were assigned at 1750 cm^{-1} . The transmission bands assigned at 1640 and 1383 cm^{-1} are endorsed to the H-O-H/ carboxylate, bending vibrations of the water molecules, respectively [14-15]. The splitting of stretching asymmetric mode of metal carbonates was confirmed by transmission bands found near 1514 and 1462 cm^{-1} [16].

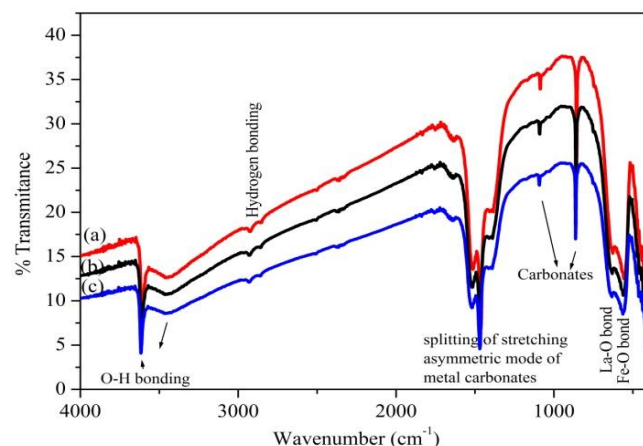


Fig. 2. FTIR spectra of lanthanum ferrite samples (a) LF1, (b) LF2 and (c) LF3

The transmission bands near 1087 and 856 cm^{-1} can be attributed to the presence of carbonates. This result is very significant for confirmation of carbonate traces which may result in porous ceramics due to elimination of CO_2 [17]. The low wavenumber side transmission bands are attributed to metallic bonds. The peaks at 557 and 627 cm^{-1} are attributed to the vibrations of Fe-O bond and La-O, respectively [18]. The stretching modes of the BO_6 octahedra of perovskite structure ABO_3 is principal cause for the existence of bands in the region 630-550 cm^{-1} . In synthesized perovskite lanthanum ferrite, the Fe-O bonds of the BO_6 octahedral units are stronger than those of the 12-coordinated La-O units, thus, one may predict that the BO_6 units dominate the spectroscopic behaviour, i.e. FeO_6 octahedral dominates over 12-coordinated La-O units [19-20]. With variation of composition, there is no major change in transmission bands only a slight change in intensity and transmission bands shifted to the higher wave number side with increasing the content of lanthanum oxide.

UV-vis Spectroscopy

Fig. 3(a-b) shows the typical UV-visible spectra of synthesized LaFeO_3 . In spectra of Fig. 3(a), the sharp intense absorption band arises to optical band gap which manifests itself as an absorption edge. Fig. 3(b) shows the Tauc plot between $\alpha^2(h\nu)$ and photon energy ($h\nu$).The

optical band gap is calculated by extrapolation of linear plot (Tauc plot) between absorption coefficient (α) and photon energy and denoted by given equation [21]:

$$\alpha(h\nu) = (h\nu - E_g)^{1/2} \quad (1)$$

where, E is the photon energy and E_g is the optical band gap energy of the material.

The above equation shows a linear dependence of $\alpha^2(h\nu)$ on photon energy (E). The optical band gap of LaFeO_3 samples was found to be 3.91 eV, 3.97 eV and 4.03 eV respectively for samples LF1, LF2 and LF3. With increasing La/Fe ratio in lanthanum ferrite, the optical band gap was found to increased. This increase in optical band is due to higher optical band gap of lanthanum oxide in comparison to ferric oxide [21-22].

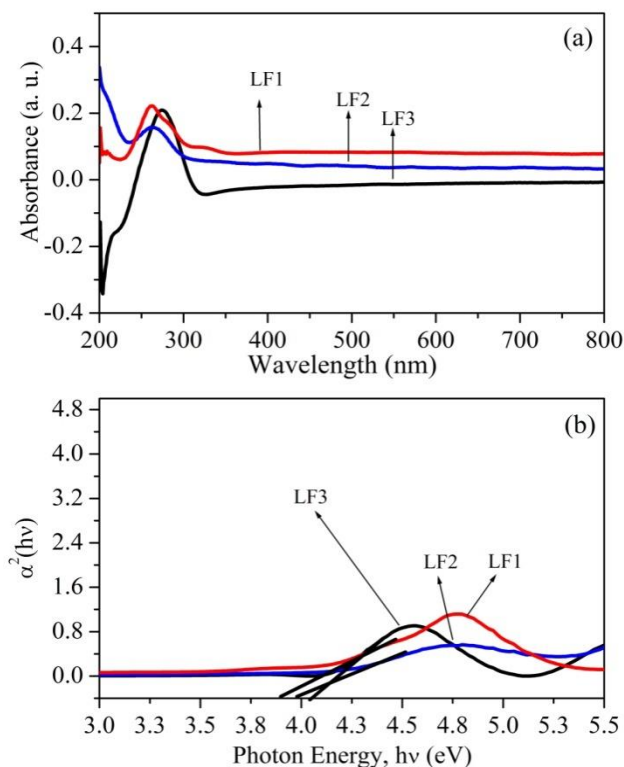


Fig. 3. (a) UV-vis spectra and (b) Tauc Plot lanthanum ferrite samples LF1, LF2 and LF3.

X-ray Diffraction

Fig. 4(a-c) shows the X-ray Diffraction patterns of prepared samples (a) LF1, (b) LF2 and (c) LF3 samples. XRD patterns were indexed with standard JCPDS file Nos. 37-1493, 65-3185 and 89-7047 for LaFeO_3 , La_2O_3 and Fe_2O_3 , respectively. These patterns clearly indicate the formation lanthanum ferrite in orthorhombic crystal structure as a major crystallite phase and La_2O_3 and Fe_2O_3 are secondary phases which are found in trace amounts. With increasing the content of lanthanum oxide, the secondary phases were minimized because lanthanum

oxide also plays the role of nucleating agent for crystallization [23]. Average crystallite size of major phase was calculated using Debye-Scherrer formula, which is follows as:

$$D = \frac{K\lambda}{\beta \cos\theta} \quad (2)$$

where, β is the full width at half maximum (FWHM) of the peak, λ is wavelength of Cu-K α X-ray, θ is the diffraction angle and $K = 0.94$, a dimensionless constant. The highest intensity peak is assigned to orthorhombic crystallite LaFeO_3 reflection. Average crystallite size of LaFeO_3 was found to be 45-50 nm. With increasing the content of lanthanum oxide, the average crystallite size was found to be decreased which is also confirmed by scanning electron microscopic results [22].

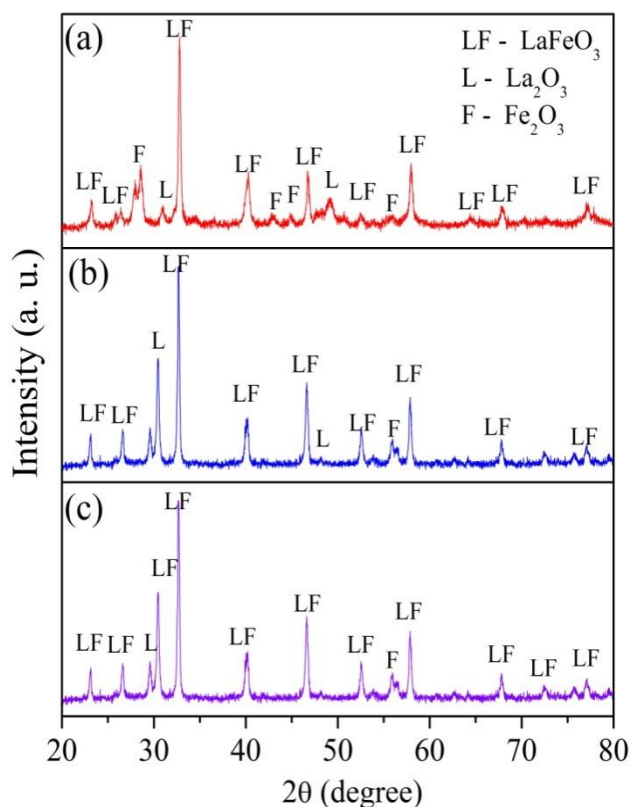


Fig. 4. XRD patterns of lanthanum ferrite samples (a) LF1, (b) LF2 and (c) LF3.

Scanning Electron Microscopy

The typical scanning electron micrographs (SEM) are shown in Fig. 5(a-c) for prepared pellet samples LF1, LF2 and LF3. From SEM images, it is clear that lanthanum ferrite crystallites were uniformly distributed in entire pellet samples. The spherical shaped uniform grain found in lanthanum ferrite is a key factor for humidity sensing application because of the surface to volume ratio.

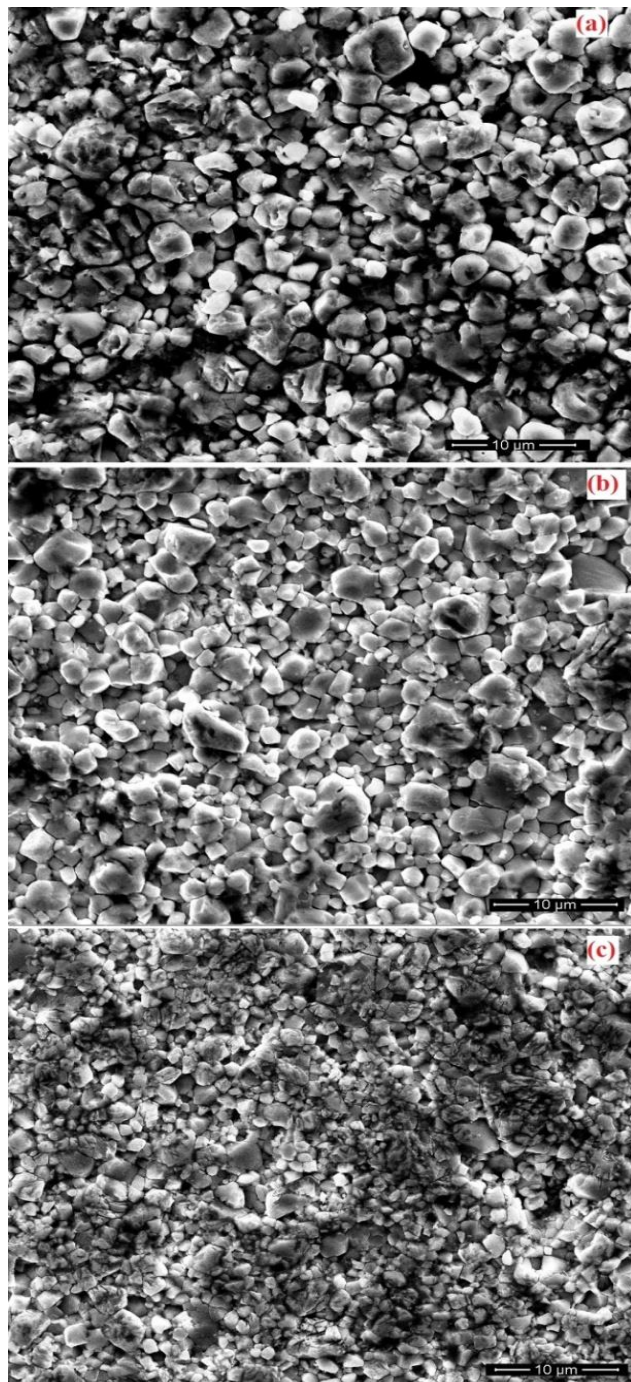


Fig. 5. SEM images of lanthanum ferrite samples (a) LF1, (b) LF2 and (c) LF3.

This happened due to the diffusion of La^{3+} ions mainly closer to the grain boundary, which exhibits ion and oxygen vacancies [24]. Each micrograph indicates the formation of pores which are attributed to release of carbonate groups as confirmed in FTIR analysis. The pores are also formed by the interconnection and distribution of crystallites. The pores in the pellet samples play the significant role humidity sensing applications. These pores act as absorption sites to adsorb water vapor.

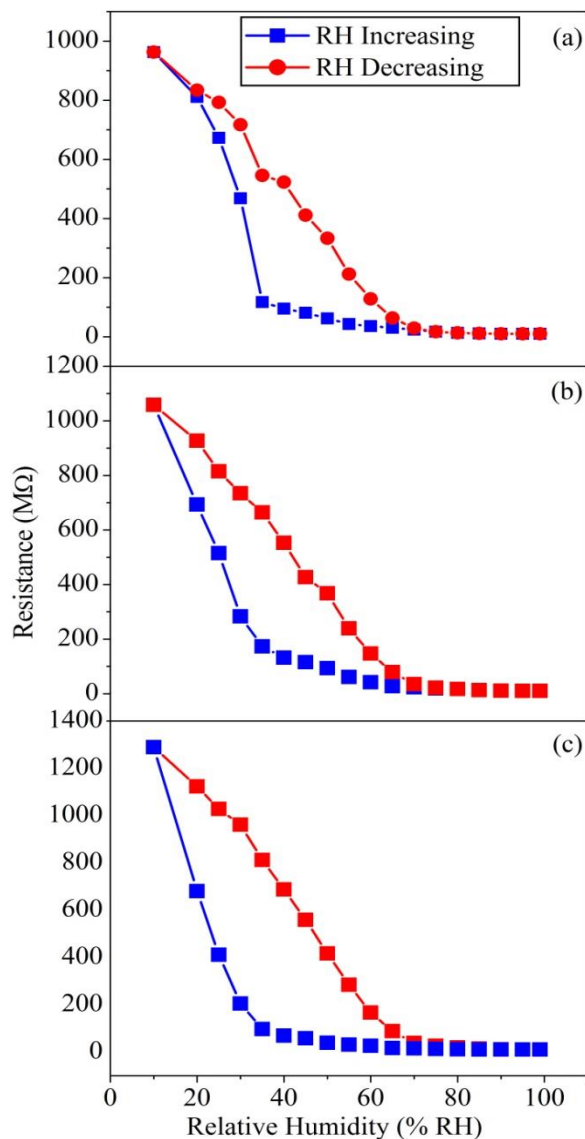


Fig. 6. Hysteresis of lanthanum ferrite samples (a) LF1, (b) LF2 and (c) LF3.

Gas Sensing Mechanism

Fig. 6(a-c) shows the variations of resistance with relative humidity at room temperatures for sensing pellets LF1, LF2 and LF3, respectively. From Fig. 6, it is clear that with increasing the relative humidity 10%-99%, the resistance decreases. Further, the resistance increases with decreasing the relative humidity from 10% to 99% but with increase and decrease of relative humidity, change in resistance does not follow the same path. This change in resistance is associated with several hysteresis loss. As relative humidity was increased, the resistance decreased sharply in the range of lower humidity i.e., from 10-30 %RH and further became constant in the range 50-99 %RH. During the decreasing of relative humidity, the resistance was found to be relatively higher than resistance when humidity was increased for the same relative

humidity. This may be due to some water vapor remaining in pores which is adsorbed during increase of relative humidity. With increasing the concentration of lanthanum oxide in perovskite lanthanum ferrite, the resistance was found to be higher. This higher resistance may be attributed to the large number of pores created by increasing the concentration of lanthanum oxide. The whole experiment is repeated in same physical environment after 3 months for samples. The humidity sensing results were found to be almost same as previous results which were conducted 3 months before. This shows the good reproducibility in lanthanum ferrite samples for humidity sensing as indicated in Fig. 7.

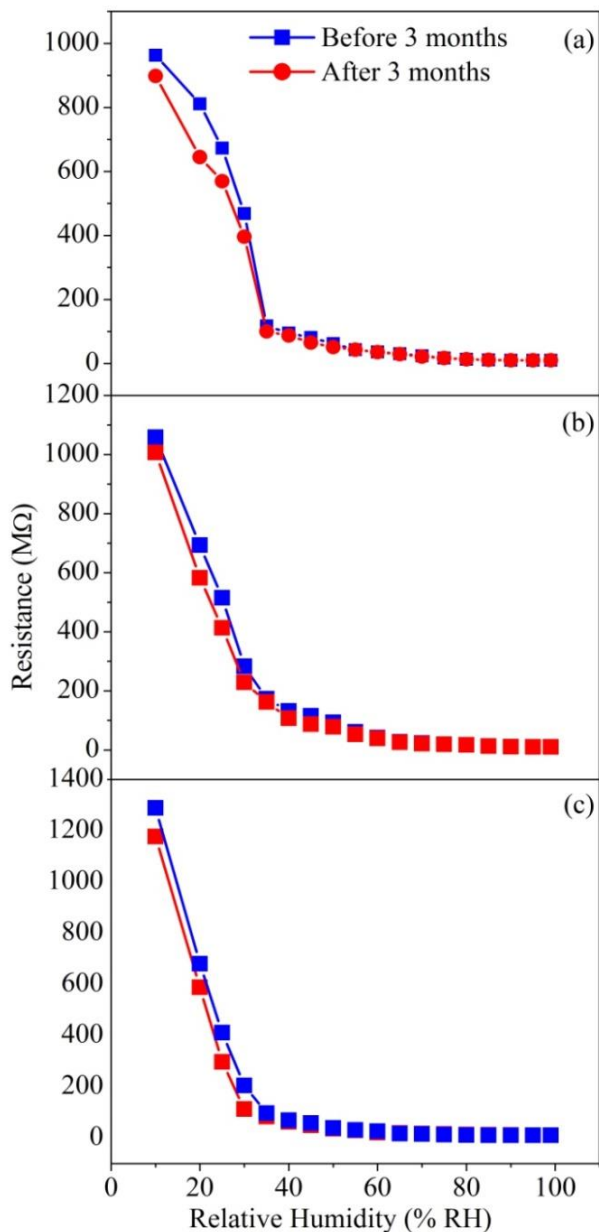


Fig. 7. Reproducibility of lanthanum ferrite samples (a) LF1, (b) LF2 and (c) LF3.

The average sensitivity is calculated by taking the average of all sensitivities ranging from 5 to 99 %RH. The average sensitivities of the pellet at room temperature were found to be 10.18 MΩ/%RH, 10.31 MΩ/%RH and 11.46 MΩ/%RH for samples LF1, LF2 and LF3, respectively as in indicated in Fig.8.

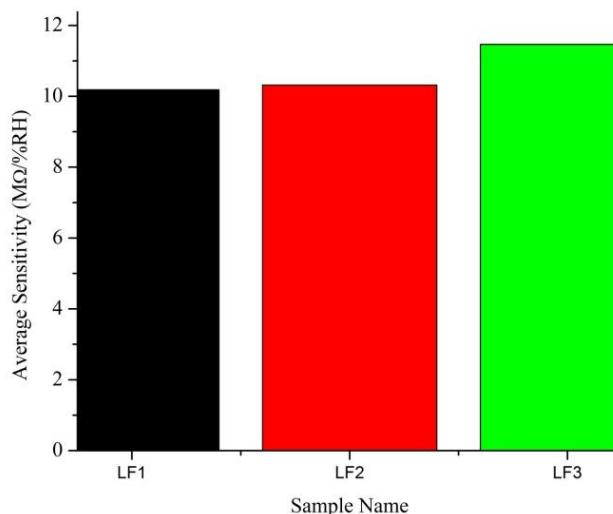


Fig. 8. Average sensitivity of lanthanum ferrite samples LF1, LF2 and LF3.

The mechanism of humidity sensing in semiconducting lanthanum ferrite samples can be understood by taking consideration of electrical response of the chemically and physically adsorbed layers of water molecules and capillary formed connecting the pores. The surface of the sensing element plays a vital role in analyzing the humidity sensing nature. The water vapor of the environment is condensed on the upper layer of the sensing element which conducts the proton from an aquatic layer [25-26]. Nan composites exhibit better sensing properties for humidity due to larger surface to volume ratio and consequently larger is the density of charge carriers usually protons.

When water vapor or humidity is exposed on sensing elements then the conductivity difference was created due to absorption of water vapor on sensing sites (pores) which leads to increase of their electrical conductivity [27-29]. In low relative humidity regions, the electrical conduction due to absorption of water vapor in the internal surfaces of porous materials dominates. Sensor operation is based on either electronic or ionic conductivity. Physisorption is basic for humidity sensing application for porous materials. In this mechanism, semiconducting surface of nanocomposite containing pores the pores adsorb the water vapor on initially chemisorbed layer of hydroxyl ions [30-31]. Grotthuss chain reaction mechanism is responsible for the conduction of protons through tunnel from one water molecule to the next via hydrogen bonding that exists universally. The high electrostatic fields near the interface of surface sensing

element and adsorbed layer breaks the physisorbed water into H_3O^+ and OH^- . The charge carriers move due to movement of protons from H_3O^+ ions to an adjacent water molecule and so on. This process sets up the protonic conduction on the surface. This charge transport mechanism is known as Grotthuss chain reaction mechanism. The increase in the conductivity due to charge transport mechanism in humid environments is the major parameter for sensors and consequently drop in resistance is noted in sensors. The surface protonic conduction is the only responsible mechanism in low humidity regions. However, electrolytic conduction also takes place in higher relative humidity, where water may condense on the sensing surface, causing a large change in resistance. Exponential dependence of resistance with relative humidity can be quantified by this mechanism.

CONCLUSION

Perovskite lanthanum ferrite nanocomposite was successfully synthesized via solid state reaction route. X-ray diffraction study confirms the clear crystallization of lanthanum ferrite as a major crystallite phase. The average crystallite size of prepared lanthanum ferrite calculated by Debye-Scherrer formula was found to be 45-50 nm. The presence of pores in samples were seen by scanning electron microscopic studies and it is validated by presence of transmission band near 856 cm^{-1} due to release of carbonate group. The optical band gap of synthesized lanthanum ferrite was found to be 3.91- 4.03 eV. It is found to increase with increasing La/Fe ratio. Prepared samples were investigated for humidity sensing application. The average sensitivity of synthesized lanthanum ferrite samples was found to be 10.18-11.46 $M\Omega/\%RH$. The resistance in low humidity region was found to be higher in comparison to higher relative humidity exposure on lanthanum ferrite samples. In the low relative humidity regions, the conduction process takes place due to sensing material but in higher relative humidity regions, the conduction of adsorbed water molecules dominates over sensing material.

ACKNOWLEDGEMENTS

The author gratefully acknowledges the Government of Uttar Pradesh for providing the financial support under 'Research and Development Scheme' wide letter no. 46/2021/603/Seventy-4-2021-4(56)/2020. Authors also acknowledge Dept. of Physics, University of Lucknow, Lucknow, Dept. of Physics, IIT (BHU) Varanasi for providing few experimental facilities.

CONFLICTS OF INTEREST

There are no conflicts to declare.

AUTHOR CONTRIBUTIONS

Sample preparation, data collection, manuscript writing is carried out by AKY.

REFERENCES

1. Zhang, Z.; Li, F.; Zheng, Y.; *Sensors and Actuators A: Physical*, **2023**, 358, 114435.
2. Zhao, J.; Liu, Y.; Li, Y.; Lu, G.; You, L.; Liang, X.; Liu, F.; Zhang, T.; Du, Y.; *Sensors and Actuators B: Chemical*, **2013**, 181, 802.
3. Chou, K.S.; Lee, T.K.; Liu, F.J.; *Sensors and Actuators B*, **1999**, 56, 106.
4. Ma, Z.; Fei, T.; Zhang, T.; *Sensors and Actuators B: Chemical*, **2023**, 376, 133039.
5. Wang, J.; Wu, F.Q.; Shi, K.H.; Wang, X.H.; Sun, P.P.; *Sensors and Actuators B*, **2004**, 99, 586.
6. Zhao, S.; Sin, J.K.O.; Xu, B.; Zhao, M.; Peng, Z.; Cai, H.; *Sensors and Actuators B*, **2000**, 64, 83.
7. Toan, N.N.; Saukko, S.; Lantto, V.; *Physica B*, **2003**, 327, 279.
8. Aono, H.; Traversa, E.; Sakamoto, M.; Sadaoka, Y.; *Sensors and Actuators B*, **2003**, 94, 132.
9. Zhang, Y.M.; Lin, Y.T.; Chen, J.L.; Zhang, J.; Zhu, Z.Q.; Liu, Q.J.; *Sensors and Actuators B: Chemical*, **2014**, 190, 171.
10. Jun, P.; Wang, Y.J.; Ji, M.; *Ferroelectrics*, **2010**, 402, 79.
11. Desai, P.A.; Athawale, A.A.; *Defence Science Journal*, **2013**, 63, 285.
12. Porter, M.D.; Bright, T.B.; Allara, D.L.; Chidsey, C.E.D.; *Journal of American Chemical Society*, **1987**, 109, 3559.
13. Gautam, C.R.; Yadav, A.K.; Singh, A.K.; *ISRN Ceramics*, **2012**, 2012, 1.
14. Sanpo, N.; Wang, J.; Berndt, C.C.; *Journal of the Australian Ceramic Society*, **2013**, 49, 84.
15. Ghosh, S.; Dasgupta, S.; *Materials Science-Poland*, **2010**, 28, 427.
16. Bhargav, K.K.; Maity, A.; Ram, S.; Majumder, S.B.; *Sensors and Actuators B*, **2014**, 195, 303.
17. Sivakumar, M.; Gedanken, A.; Zhong, W.; Jiang, Y.H.; Du, Y.W.; Brukental, I.; Bhattacharya, D.; Yeshurunc, Y.; Nowik, I.; *Journal of Materials Chemistry*, **2004**, 14, 764.
18. Thuy, N.T.; Minh, D.L.; *Advances in Materials Science and Engineering*, **2012**, 2012, 1.
19. Lavat, A.E.; Baran, E.J.; *Vibrational Spectroscopy*, **2003**, 32, 167.
20. E.K.A. Khalek, H.M. Mohamed, *Hyperfine Interact*, **2013**, 222, S57.
21. Singh, S.; Singh, A.; Wan, M.; Yadav, R.R.; Tandon, P.; Rasool, S.S.A.; Yadav, B.C.; *Sensors and Actuators B*, **2014**, 205, 102.
22. Humayun, M.; Ullah, H.; Usman, M.; Yangjeh, A.H.; Tahir, A.A.; Wang, C.; Luo, W.; *Journal of Energy Chemistry*, **2022**, 66, 314.
23. Song, J.; Lu, C.; Xu, D.; Ni, Y.; Liu, Y.; Xu, Z.; Liu, J.; *Polymer international*, 2010, 59, 954.
24. Rajeshwari, A.; Punithavathy, I.K.; Jeyakumar, S.J.; Lenin, N.; Vigneshwaran, B.; *Ceramics International*, **2020**, 46, 6860.
25. Chowdhri, A.; Sharma, P.; Gupta, V.; Sreenivas, K.; Rao, K.V.; *J. Appl. Phys.*, **2002**, 92, 2172.
26. Cosentino, I. C.; Muccillo, E. N. S.; Muccillo, R.; *Materials Chemistry and Physics*, **2007**, 103, 407.
27. Chen, G. Fu, H.; Chen, Z.; Zhang, J.; Kohler, H.; *Sens. Actuators B*, **2002**, 81, 308.
28. Anderson, J. H.; Parks, G. A.; *J. Phys. Chem.*, **1968**, 72, 3362.
29. McCafferty, E.; Zettlemoyer, A.C.; *Disc. Faraday Soc.*, **1971**, 52, 239.
30. Traversa, E.; *Sens. Actuators B*, **1995**, 23, 135.
31. Fleming, W. J.; *Society of automotive e engineers transactions*, **1981**, 90, 1656.

Authors Biography



Dr. Avadhesh Kumar Yadav serves as Assistant Professor in Dept. of Physics, F.A.A. Govt. PG College, Mahmudabad Sitapur. Dr. Yadav has been actively involved in Materials Science, Nanotechnology and glass/ glass ceramics research for high energy storage and sensing devices since 2010. He has published more than 50 research articles in journal of international repute including 4 review articles and 5 books. The citation of his research articles are more than 1970 since November 2023. He is also editor/ associate editor of Frontiers of Public Health, Current Chinese Science, Coroviruses, Ceramic science and engineering. He has reviewed research articles for more than 80 international journals of Elsevier, Springer, Wiley, Taylor & Francis, Nature, ACS, RSC etc.



This article is licensed under a Creative Commons Attribution 4.0 International License, which allows for use, sharing, adaptation, distribution, and reproduction in any medium or format, as long as appropriate credit is given to the original author(s) and the source, a link to the Creative Commons license is provided, and changes are indicated. Unless otherwise indicated in a credit line to the materials, the images or other third-party materials in this article are included in the article's Creative Commons license. If the materials are not covered by the Creative Commons license and your intended use is not permitted by statutory regulation or exceeds the permitted use, you must seek permission from the copyright holder directly.

Visit <http://creativecommons.org/licenses/by/4.0/> to view a copy of this license

Graphical Abstract

In graphical abstract the synthesis method of lanthanum ferrite via solid state reaction route is represented. Moreover, one SEM image shows the pores which plays important role in humidity sensing applications.

